

Self-Assembled Chains and Solids of Dipolar Atoms in a Multilayer

G. Guijarro,^{1,2} G. E. Astrakharchik,¹ G. Morigi,² and J. Boronat¹

¹*Departament de Física, Campus Nord B4-B5, Universitat Politècnica de Catalunya, E-08034 Barcelona, Spain*

²*Theoretische Physik, Universität des Saarlandes, Campus E2.6, D-66123 Saarbrücken, Germany*

(Dated: March 21, 2024)

We predict that ultracold bosonic dipolar gases, confined within a multilayer geometry, may undergo self-assembling processes, leading to the formation of chain gases and solids. These dipolar chains, with dipoles aligned across different layers, emerge at low densities and resemble phases observed in liquid crystals, such as nematic and smectic phases. We calculate the phase diagram using quantum Monte Carlo methods, introducing a newly devised trial wave function designed for describing the chain gas, where dipoles from different layers form chains without in-plane long-range order. We find gas, solid, and chain phases, along with quantum phase transitions between these states. Specifically, we predict a quantum phase transition from a gaseous to a self-ordered phase, which occurs at a critical interlayer distance. Remarkably, in the self-organized phases, the mean interparticle distance can significantly exceed the characteristic length of the interaction potential, yielding solids and chain gases with densities several orders of magnitude lower than those of conventional quantum solids.

Introduction. Self-assembled systems in ultracold atoms represent a fascinating and rapidly evolving area of research at the intersection of atomic physics, quantum optics, and condensed matter physics. Among the intriguing systems in this context are dipolar chain gases and solids, in which atoms with large magnetic or electric dipole moments interact with each other via long-range and anisotropic dipolar interactions, leading to the spontaneous formation of ordered structures. These self-assembled systems can exhibit a variety of exotic quantum effects, including dipolar quantum droplets [1–9], roton excitations in dipolar condensates [10–12], and dissociation of a dipolar chain crystal [13].

Recent experiments with ultracold atomic gases have achieved significant advances in the observation of self-organized systems, such as solids with superfluid properties (supersolids) observed in platforms with spin-orbit coupling [14] and long-range cavity-mediated interactions [15]. Although in those setups spatial translational symmetry is broken, actually the crystal periodicity is externally imposed either by optical lattices or cavities. This limitation was recently surpassed in experiments with dipolar quantum gases, which reported a spontaneous formation of crystals of droplets [4, 16, 17]. The realization of a quantum self-assembled system, in which continuous translational symmetry is naturally broken, remains an open challenge within the community of ultradilute gases.

A relevant question that arises is if stable quantum solids and chains can be spontaneously formed at ultradilute densities, where the mean interparticle distance is much larger than the range of the potential? This scenario is unusual in condensed matter, where solid phases typically occur at high densities (a notable exception is that of Wigner crystals [18] formed at low density, however, quantum effects are typically small). While there have been studies on low-density dipolar chains, previous

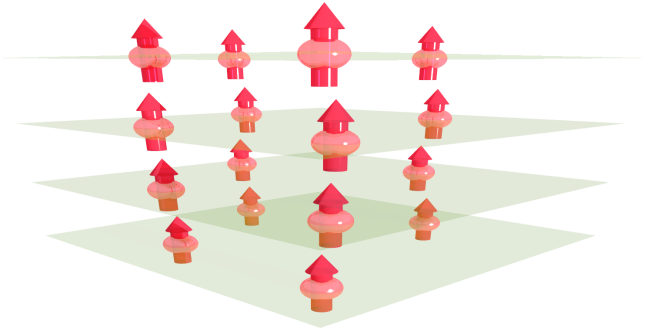


FIG. 1. Schematic view of dipoles confined to several two-dimensional layers. The dipoles are assumed to be aligned perpendicularly to the planes by an external field. In the dipolar chain phase, there exists an ordering across the planes, as dipoles from different layers form chains, without in-plane long-range order.

research either neglected interactions between chains [19] or restricted themselves to the regime of small spatial fluctuations, about the crystal phase [13]. As a result, complete description of self-assembled systems at ultradilute densities is still missing.

In the present work, we propose a possible physical realization of quantum self-assembled states. The platform consists of a system of dipolar bosons confined to a multilayer geometry, as schematically shown in Fig. 1. Using exact many-body quantum Monte Carlo techniques [20–22] and proposing a novel trial wave function tailored specifically to model chain gases, we determine the ground-state phase diagram when the dipoles are all aligned perpendicularly to the parallel layers by an external field. We anticipate the emergence of a stable phase characterized by self-organized chains across layers when the density is low. We find a quantum phase transition from a gas to an ordered phase, solid or chains, as the interlayer distance decreases. Remarkably, the density of

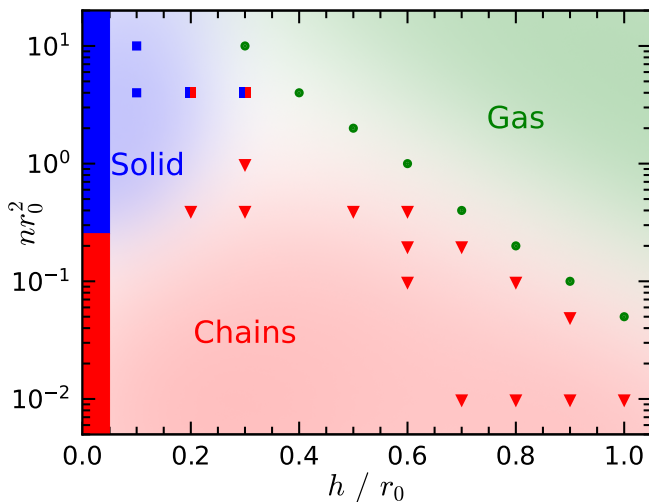


FIG. 2. Ground-state phase diagram of dipolar bosons confined to a four-layer system at zero temperature, as a function of the total density nr_0^2 and the separation between layers h/r_0 . We have identified three phases: gas, solid, and chains. In the limit of $h/r_0 \rightarrow 0$, the low-density chain phase (indicated with a red bar) experiences a phase transition to a solid state (indicated with a blue bar) at the critical density $n_c r_0^2 \approx 0.283$.

the self-assembled phases is several orders of magnitude lower than the one of conventional quantum solids.

Hamiltonian. We consider N bosons of mass m and dipole moment d constrained by a multilayer geometry composed of M two-dimensional (2D) parallel layers, each separated by a distance h . We assume that each layer contains the same number (N/M) of dipoles and that the interlayer tunneling is suppressed so that the transverse degrees of freedom are frozen. The dipolar moments are considered to be oriented perpendicularly to the 2D planes, which can be achieved by applying a polarizing field. The Hamiltonian of this system is given by the sum of the kinetic energy operator and the dipolar interaction potential,

$$H = -\frac{\hbar^2}{2m} \sum_{i=1}^N \nabla_i^2 + d^2 \sum_{i<j}^N \frac{|\mathbf{r}_i - \mathbf{r}_j|^2 - 2(l_i - l_j)^2 \hbar^2}{(|\mathbf{r}_i - \mathbf{r}_j|^2 + (l_i - l_j)^2 \hbar^2)^{5/2}}. \quad (1)$$

Here, \mathbf{r}_i denotes (x, y) coordinates of particle i in one of M planes with $l_i = 1, 2, \dots, M$ being the index of the plane. For dipoles in the same layer, $l_i = l_j$, the dipolar interaction is always repulsive and falls off with a power law $1/r^3$. For dipoles in different layers, $l_i \neq l_j$, the dipolar interaction is attractive for small values of r but repulsive for large values of r , where r is the in-plane distance between dipoles. In the following, we use the dipolar length $r_0 = md^2/\hbar^2$ as a unit of length. A further characteristic length is the interlayer distance h : a dipole at the origin of the layer $l_i = 1$ experiences an attractive interaction with atoms at the l_j layer within a cone of radius equal to $\sqrt{2}|l_i - l_j|h$.

Quantum Monte Carlo Simulations. The ground-state properties of the system, described by the Hamiltonian (1), are calculated using the diffusion Monte Carlo (DMC) method [20–22]. The DMC method has been shown to give an accurate description of correlated quantum systems [23]. The DMC method solves stochastically the many-body Schrödinger equation in imaginary time resulting in an exact value (within controllable statistical error) of the ground-state energy, alongside other properties. We use guiding wave functions to impose a specific symmetry to the state and to improve the convergence. To characterize the gas phase, we use a trial wave function in Bijl-Jastrow (BJ) form, which maintains translational symmetry and consists of two-body correlation terms. Conversely, for the solid phase, we adopt a Nosanow-Jastrow (NJ) wave function. This NJ form incorporates one- and two-body correlation factors, thus breaking translational symmetry (see Supplemental Material (SM)). The positions of the dipoles confined to the multilayer geometry are projected into a box of size $L_x \times L_y$ and periodic boundary conditions along (x, y) plane are used to simulate the bulk system. The total density is defined as $n = N/(L_x L_y)$.

In addition to the gas and solid phases, the presence of anisotropic interactions allows for the emergence of a dipolar chain phase. This phase is similar to the molecular phase observed in bilayer systems [24–26] but extends beyond two layers. While the use of BJ (for gas) and NJ (for crystal) trial functions is well-established in the literature, to the best of our knowledge, a Monte Carlo description for dipolar chain systems is still lacking. Here, we propose a new type of trial wave function specifically designed to describe chain phases. Its primary characteristic lies in not only capturing interlayer correlations but also enabling the free movement of chains within planes. We found that the chain trial wave function results in lower energy in certain regions of the phase diagram compared to the trial wave functions for solids and gases. Therefore, the novel introduction of the chain trial wave function is essential for fully describing the phase diagram of the dipolar multilayer system (see SM).

Ground state of dipolar bosons within a four-layer system. To construct the phase diagram, we explored the parameter space and calculated the ground-state energy using three different trial wave functions. To verify which phase has the lowest energy, we calculate the DMC energy E_{DMC} , add the tail energy correction E_{tail} , and extrapolate the corrected value to the thermodynamic limit, E_{th} , as discussed in the SM. The resulting phase diagram is reported in Fig. 2 as a function of two key parameters: the dimensionless density nr_0^2 and the separation between layers h/r_0 . An important observation is the existence of the chain phase which spans across a wide range of interlayer distances. Its large extension enhances the feasibility of its experimental observation.

Furthermore, this phase extends to extremely low densities, at which the mean interparticle distance within one layer can range from 1 to 20 times larger than the dipolar length r_0 , resulting in the formation of atomic dipolar chains at ultradilute density.

At small interlayer distances $h/r_0 < 0.2$, we observe the appearance of the solid phase as the density increases, above the crystallization density of approximately $n_c r_0^2 \approx 0.283$. Additionally, for interlayer distances larger than $h/r_0 > 0.4$, we observe a quantum phase transition from chains to gas as the density increases. Remarkably, for certain densities ($n r_0^2 \approx 1$), the change in h/r_0 induces a series of phase transitions crossing gas, chain, and solid phases as the distance between the layers is decreased. We provide estimates for the boundaries of the gas phase, along with the transition line from chains to gas. However, determining the precise location of the transition from chains to solid is computationally challenging due to the similar energies of these phases across a broad parameter range.

Various phases exhibit significantly different spatial distribution of dipoles, as quantified by the pair distribution function $g(r, l)$, which indicates the probability of finding two atoms at a relative distance r and separated by l layers. In Fig. 3, we show characteristic examples of the pair distribution functions $g(r, l)$ in the gas (a), solid (b), and chain (c) phases.

The same-layer distribution $g(r, l = 0)$ vanishes at short distances due to the strongly repulsive hard core of the dipolar potential at $r/r_0 \rightarrow 0$. In the gas phase, the in-layer correlation function exhibits a shallow maximum and then approaches the unit value, i.e., the asymptotic value of uncorrelated atoms, see Fig. 3a. However, correlation functions between different layers ($l > 0$) show a notably distinct short-range behavior. In particular, there is a high peak in $g(r, l > 0)$ at $r/r_0 = 0$ as a result of the maximum interlayer attraction between the dipoles in adjacent layers. As the distance r increases, $g(r, l > 0)$ exhibits a minimum, and eventually approaches its uncorrelated value of 1. A representative snapshot of the atom positions in the gas phase in the DMC simulations is presented in Fig. 3d and it shows that the dipoles are uniformly distributed without any specific pattern.

Characteristic examples of the pair distribution functions in the solid phase are also shown in Fig. 3b. At short distances, $r \rightarrow 0$, the behavior is similar to that observed in the gas phase, where the same-layer distribution vanishes as dipoles approach each other, while different-layer distributions exhibit a pronounced correlation peak. As distance r increases, the solid pair distributions show stronger correlations compared to the gas phase, as a result of the spatial ordering in the solid. Consequently, $g(r, l)$ displays several pronounced oscillations in a solid phase, whereas in the gas phase, it rapidly converges to the uncorrelated values of $g(r, l) = 1$. The amplitude of these oscillations depends on the system parameters. In

a triangular lattice, the first peak is particularly prominent, corresponding to six neighbors located at the lattice spacing $r \approx a_{\text{latt}}$, which is proportional to the mean interparticle distance $a_{\text{latt}} = (2/\sqrt{3})^{1/2} r_m \approx 1.075 r_m$ and is determined by the in-layer density, $r_m = \sqrt{M/n}$. In Fig. 3e, a snapshot of the atom coordinates during the DMC simulation of the solid phase is presented, revealing the periodic structure of a triangular lattice.

In Fig. 3c, we report the pair distribution functions $g(r, l)$ for the chain phase. We observe intermediate features, where some aspects resemble those of a gas phase while others are closer to those of a crystal phase. Specifically, the in-plane pair distribution $g(r, l = 0)$ shows correlations typical of the gas phase, indicating no long-range order within the layer. However, the off-plane pair distributions $g(r, l > 0)$ exhibit high peaks at short distances, similar to the strong inter-layer correlations observed in the solid phase. The snapshots of the atom coordinates during the DMC simulation, shown in Fig. 3f, provide insight into the structure of this unconventional phase. Here, the dipolar chains are uniformly distributed without forming a regular structure, indicating the absence of positional order. However, the dipoles forming the chains exhibit strong correlations in the direction perpendicular to the planes. This behavior resembles that of a nematic phase in liquid crystals.

Quantum phase transition: from gas to a self-ordered phase. The effect of different number of layers (from one to ten) on the phase diagram is summarized in Fig. 4, where the schematic phase diagram of the multilayer system is shown as a function of the dimensionless density $n r_0^2$ and the separation between layers h/r_0 . The thick horizontal lines for small h/r_0 correspond to the critical freezing density $n_c r_0^2 = 290/M^5$, indicating the density at which an M -layer system of dipolar bosons will form a crystal of super-dipoles (where all dipoles align perfectly at each point) when the interlayer separations are extremely small $h \rightarrow 0$ (see SM). Notably, this estimation of the freezing point shows that the freezing density decreases as $1/M^5$ with the number of planes M . This strong dependence on M suggests that the multilayer geometry offers a very promising setup for observing quantum solids with low surface densities in future experiments. This finding is significant because increasing the number of planes in the system can yield a very dilute solid, especially in situations characterized by small interlayer distances.

The phase diagram shown in Fig. 4 also reports an approximate threshold density $n_t r_0^2 = M/[2(M-1)^2 h^2]$ (shown with dashed lines) as a function of the interlayer separation for different number of planes (as discussed in the SM). The position of the threshold, $n_t r_0^2$, is defined as the density at which the classical interaction between particles in the top and bottom layers changes its sign at the mean interparticle distance. Densities larger (smaller) than this threshold favor the formation of a

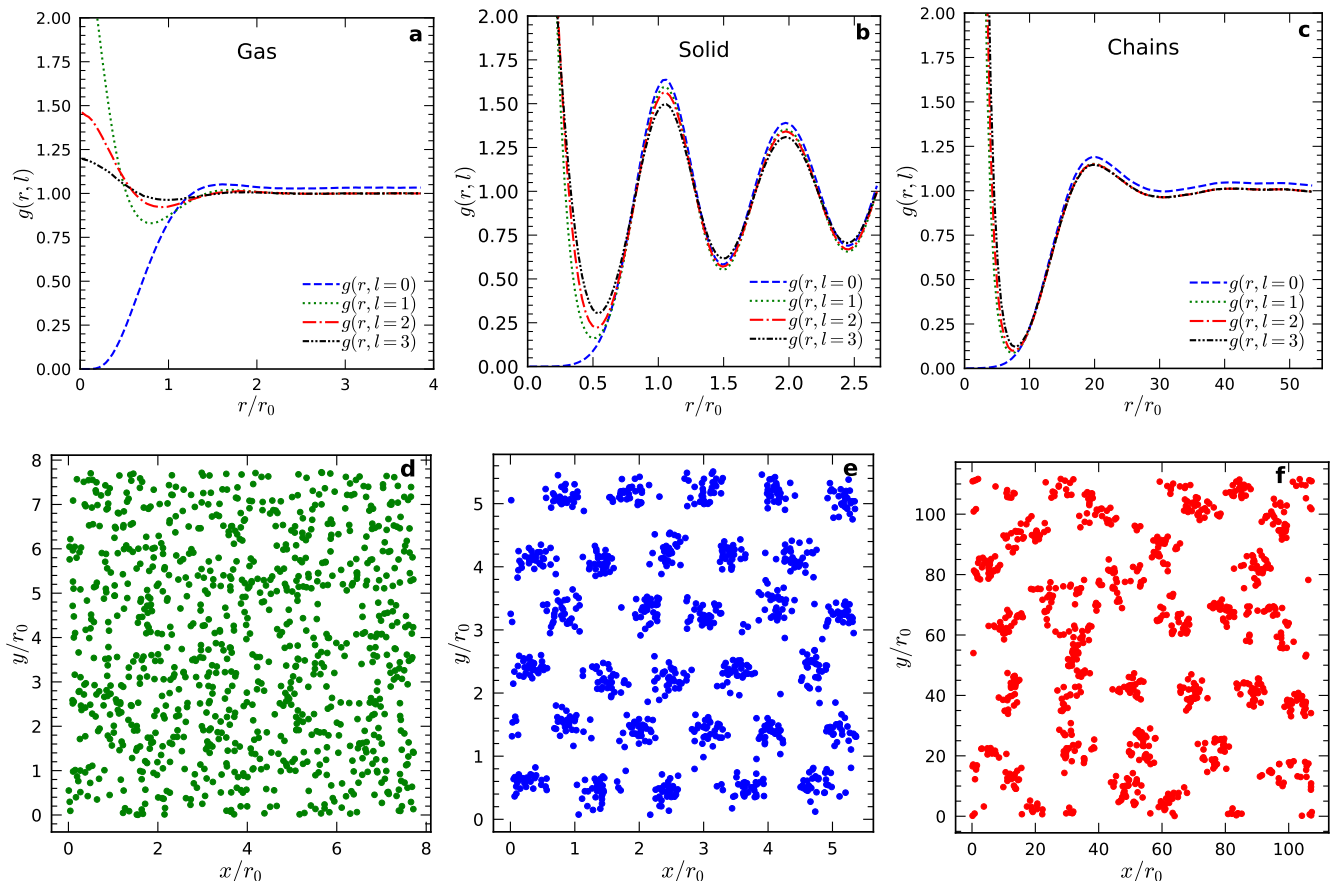


FIG. 3. Top panel: Typical in-plane $g(r, l = 0)$ and off-plane $g(r, l > 0)$ pair distribution functions in the gas (a), solid (b), and chain (c) phases within a four-layer geometry. Bottom panel: Characteristic snapshots of the atom coordinates from DMC simulations in the gas (d), solid (e), and chain (f) phases. The parameters are: gas $nr_0^2 = 2.0$, $h/r_0 = 0.5$; solid $nr_0^2 = 4.0$, $h/r_0 = 0.3$; chain $nr_0^2 = 0.01$, $h/r_0 = 0.9$.

gas (self-ordered) phase. According to this estimate, a self-ordered phase can occur at very low densities, not only for small interlayer distances but also across a wide range of separations. To support these crude estimates, we performed DMC simulations.

Using the DMC method, we observed a quantum phase transition from a gas to an ordered phase (solid or chains) as the interlayer distance decreased. To determine the critical interlayer values for this transition, we fixed the number of planes M and the total density nr_0^2 , and then systematically reduced the interlayer distance while keeping the density constant. We calculated the ground-state energy using both gas and ordered (solid or chains) trial wave functions. The phase at each point corresponds to the phase with the lowest energy. The critical interlayer distance corresponds to the value at which the phase changes from gas to an ordered phase. The estimated critical interlayer distances for the gas-ordered transition are reported in the phase diagram of Fig. 4, covering the range of layers from $M = 2$ up to 10. For each M value, the critical interlayer distance is reported

for one density. One might notice that the simple approximation of the threshold density $n_{tr}r_0^2$ becomes less accurate as M increases. Remarkably, the self-ordered phase exists across a broad range of densities and interlayer separations. Adjusting the number of planes can alter the density of the phase significantly, decreasing from $nr_0^2 = 10$ to 0.001 as the number of layers increases from $M = 2$ to 10. These extremely low densities correspond to mean interparticle distances ranging from 0.4 to 100 times the dipolar length r_0 . Moreover, the range of interlayer distances where the self-assembled phase is stable expands with the number of layers, which suggests the possibility of its experimental realization.

Feasible experimental parameters. Recently, an experimental realization of a stack of dysprosium bilayer arrays with adjustable interlayer distances has been achieved [27]. This development sets the stage for the observation of our findings. Therefore, an ultradilute quantum self-assembled dipolar system can be achieved using magnetic dipolar molecules such as $^{164}\text{Dy}_2$ [28] and $^{168}\text{Er}^{164}\text{Dy}$ [29], which have dipolar lengths of approxi-

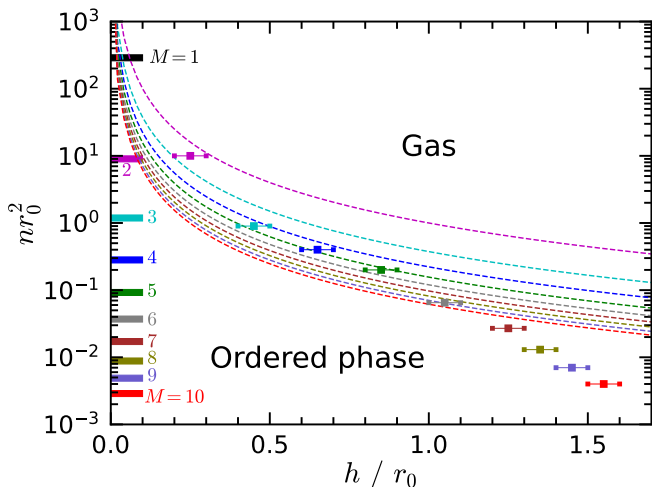


FIG. 4. Phase diagram for various number of layers ($M = 1, \dots, M = 10$) as a function of the total density nr_0^2 and the separation between layers h/r_0 . Quantum phase transition from a gas to a self-ordered phase occurs as the interlayer distance decreases. The squares indicate DMC predictions for the gas-ordered phase transitions, considering a single value of density nr_0^2 for each number of layers M and changing interlayer separation h . The crystallization $n_c r_0^2$ and threshold $n_t r_0^2$ densities are shown by the thick and dashed lines, respectively.

mately $r_0 \sim 2 \times 10^{-7}$ m and $r_0 \sim 1 \times 10^{-7}$ m, respectively. Alternatively, mixtures of bosonic dipolar molecules like $^{87}\text{Rb}^{133}\text{Cs}$ [30, 31] and $^{23}\text{Na}^{87}\text{Rb}$ [32, 33] can also be utilized, with dipolar lengths around $r_0 \sim 5 \times 10^{-6}$ m and 2×10^{-5} m, respectively. Typical experimental values for the interlayer distance, equivalent to one-half of the laser wavelength $\lambda/2$, fall within the range $h \approx (2-5) \times 10^{-7}$ m.

Conclusions. We used the diffusion Monte Carlo method to obtain the phase diagram of two-dimensional dipolar bosons confined within a multilayer geometry at zero temperature. Our findings indicate the possibility of generating self-assembled phases, such as solid and chains, at ultra-low densities. Remarkably, the density of these systems can be several orders of magnitude lower than that of conventional solids. Moreover, the freezing density can be further decreased by increasing the number of layers. Our results present a novel example of quantum dipolar self-ordered phases characterized by ultradilute density. In the solid phase, unlike previous realizations, the dipolar interactions by themselves are sufficient to create the crystalline structure, which consists of individual atoms rather than clusters. Whether this crystal exhibits a finite superfluid signal and qualifies as a new supersolid remains a topic for future research.

We gratefully acknowledge the fruitful discussions with Joaquim Casulleras. We acknowledge financial support from Ministerio de Ciencia e Innovación MCIN/AEI/10.13039/501100011033 (Spain) under Grant No. PID2020-113565GB-C21 and from

AGAUR-Generalitat de Catalunya Grant No. 2021-SGR-01411. GG and GM acknowledge partial support by the Deutsche Forschungsgemeinschaft (DFG, German Research Foundation), with the CRC-TRR 306 “QuCoLiMa”, Project-ID No. 429529648. GG acknowledges funding from the European Union, the Spanish Ministry of Universities and the Recovery, Transformation and Resilience Plan through a grant from Universitat Politècnica de Catalunya.

SUPPLEMENTAL MATERIAL

DIFFUSION MONTE CARLO METHOD

The ground-state properties of the system are calculated using the diffusion Monte Carlo (DMC) method (for details of the method see, for example, Refs. [20–22]). This method has demonstrated its capacity to provide an accurate description of correlated quantum systems [23]. Examples include ultradilute bosonic [34, 35] and fermionic mixtures [36], few and many-bosonic bound-states [26, 37], Bose [38] and Fermi [39] polarons, dipolar Bose supersolid stripes [40], Bose gas subject to a multi-rod lattice [41], and ultracold quantum gases with spin-orbit interactions [42]. The DMC method solves the many-body Schrödinger equation in imaginary time, yielding a precise estimation of the ground-state energy within controllable statistical error. By using guiding wave functions, it is possible to impose a certain symmetry characteristic for a given phase and study phase transitions. Also, the use of guiding wave functions acts as importance sampling, meaning that the more relevant regions of phase space are better sampled, minimizing the variance and the statistical error. To describe the gas phase we chose a translationally invariant trial wave function in Bijl-Jastrow (BJ) form, composed as a pair product of two-body correlation terms, while for the solid phase we used a Nosanow-Jastrow (NJ) wave function, incorporating one- and two-body correlations factors and breaking the translational symmetry. To describe the chain phase we introduce a new trial wave function, combining two-body correlation terms with many-body terms.

Trial wave function: Gas phase

To describe the gas phase we chose a trial wave function of the Bijl-Jastrow form, composed as a pair product of two-body correlations terms

$$\Psi_G(\mathbf{r}_1, \dots, \mathbf{r}_N) = \prod_{i < j}^N f_2(|\mathbf{r}_i - \mathbf{r}_j|). \quad (2)$$

The two-body terms $f_2(r)$ depend on the distance between a pair of atoms $r_{ij} = |\mathbf{r}_i - \mathbf{r}_j|$. Here, the two-body terms $f_2(r)$ are taken as the solution of the two-body problem at short distances. This solution depends on whether the dipoles are in the same layer or not. For dipoles in the same layer, we chose the short-distance part of the two-body correlations term as

$$f_2(r) = C_1 K_0 \left(2\sqrt{R_0 r_0 / r} \right), \quad (3)$$

up to R_{match} . Here $K_0(r)$ is the modified Bessel function, R_{match} and R_0 are variational parameters.

For distances larger than R_{match} we chose the two-body correlation function as

$$f_2(r) = C_2 \exp \left[-\frac{C_3}{r} + \frac{C_3}{r-L} \right], \quad (4)$$

which take into account the contributions from other particles and describe long-range phonons in the form established by Reatto and Chester [43]. The coefficients C_1 , C_2 , and C_3 are fixed by imposing continuity of the function and its first derivative at the matching distance R_{match} , and also that $f_2(L/2) = 1$.

For dipoles in different layers, the interlayer correlations are taken as the solution of the two-body problem $f_2(r)$ up to R_1 . We also impose the boundary condition $f_2(R_1) = 0$. For distances larger than the variational parameter $0 < R_1 < L/2$ we set $f_2(r) = 1$.

Trial Wave Function: Solid phase

We use the standard Nosanow-Jastrow trial wave function to describe the solid phase [44]

$$\Psi_S(\mathbf{r}_1, \dots, \mathbf{r}_N; \{\mathbf{R}_I^c\}) = \prod_{j < k}^N f_2(|\mathbf{r}_j - \mathbf{r}_k|) \prod_{i=1}^N f_1(|\mathbf{r}_i - \mathbf{R}_i^c|), \quad (5)$$

where \mathbf{r}_i are the positions of the atoms, $\{\mathbf{R}_I^c\}$ are the positions defining the equilibrium crystal lattice, and $f_1(r)$ and $f_2(r)$ are the one-body and two-body correlation factors, respectively.

The two-body correlation functions $f_2(r)$ used in Ψ_S are of the same form as those used to describe the gas phase Ψ_G , although the specific values of the variational parameters might differ.

The one-body terms $f_1(r)$ localizes each atom close to its lattice site and are modeled by a Gaussian function

$$f_1(r_i) = e^{-\alpha|\mathbf{r}_i - \mathbf{R}_i^c|^2}, \quad (6)$$

where α is the localization strength and R_i^c is the position of the lattice site. Notice that in our case, R_i^c are fixed by the triangular lattice. Meanwhile, α is a variational parameter, which is chosen by minimizing the variational energy.

Trial wave function: Chain Gas phase

A single chain consists of M dipoles, each belonging to a different layer without any crystal ordering between them. These chains are flexible but will not become tangled due to repulsive forces between dipoles in the same layer. To describe the chain phase, we construct a trial wave function by combining two-body correlation terms $f_2(r)$, which depend on the distance between a pair of atoms $r_{jk} = |\mathbf{r}_j - \mathbf{r}_k|$, with many-body terms $f_M(|\mathbf{r}_i - \mathbf{R}_i|)$, depending on the position of an atom \mathbf{r}_i and the center of mass of the chain \mathbf{R}_i (which depends on the positions of atoms in the same chain).

$$\Psi_C(\mathbf{r}_1, \dots, \mathbf{r}_N) = \prod_{j < k}^N f_2(|\mathbf{r}_j - \mathbf{r}_k|) \prod_{i=1}^N f_M(|\mathbf{r}_i - \mathbf{R}_i|). \quad (7)$$

For the two-body functions $f_2(r)$ we maintain the same structure as in the gas and solid phases, although the specific values of the variational parameters are generally different. We consider the many-body terms $f_M(r)$ of a Gaussian shape,

$$f_M(r_i) = e^{-\alpha|\mathbf{r}_i - \mathbf{R}_i|^2}, \quad (8)$$

where the variational parameter α quantifies the strength of localization. The chain center of mass is defined as

$$\mathbf{R}_i = \frac{1}{M} \sum_{k \in C_i} \mathbf{r}_k, \quad (9)$$

with the sum covering all atoms belonging to the same chain as the i -th atom. The function $f_M(r)$ is a many-body term, as a displacement of a single atom leads to M changes in the function due to the resulting movement of the center of mass. A crucial difference between the solid and chain trial wave functions is that the positions of the lattice sites \mathbf{R}_i in the NJ function remain static and are fixed by the triangular lattice whereas they change in Ψ_C during the simulation. We found that using the chain trial wave function Ψ_C lowers the energy in specific parts of the phase diagram compared to the trial wave functions used for solids and gases. This means that introducing the chain trial wave function is crucial for accurately describing the phase diagram of the dipolar multilayer system (further details of this trial wave function can be found in Ref. [45]).

Freezing density

In Ref. [46], the authors studied the ground-state phase diagram of a two-dimensional Bose system with dipole-dipole interactions using the QMC methods. The dipoles were constrained to move in a single plane and were polarized in the perpendicular direction to the plane. The

authors found a quantum phase transition from a gas to a solid phase as the density increases. This transition was estimated to occur at the critical density $\tilde{n}\tilde{r}_0^2 \approx 290$, with $\tilde{r}_0 = r_0 = md^2/h^2$ and $\tilde{n} = n$ for a single layer of dipoles.

Now, we show how $\tilde{n}\tilde{r}_0^2 \approx 290$ is rewritten for a system with M layers in the limit of rigid chains. To do this, consider a chain with M dipoles, one in each layer. When $h \rightarrow 0$ the chain becomes a super-dipole with mass Mm , dipolar moment Md , and dipolar length

$$\tilde{r}_0 = \frac{(Mm)(Md)^2}{h^2} = M^3 r_0. \quad (10)$$

Now, consider an M -layer system with N dipoles and N/M chains evenly distributed. When $h \rightarrow 0$ the M -layer system effectively becomes to a single-layer one, each chain becomes a super-dipole, and the number of particles changes from N dipoles to N/M super-dipoles. As a consequence of the latter the density now is given by $\tilde{n} = n/M$, and in dipolar units it becomes

$$\tilde{n}\tilde{r}_0^2 = \left(\frac{n}{M}\right) (M^3 r_0)^2 = M^5 n r_0^2. \quad (11)$$

From the last relation and with $\tilde{n}\tilde{r}_0^2 \approx 290$ we obtain

$$n_c r_0^2 = \frac{290}{M^5}. \quad (12)$$

In the limit of $h \rightarrow 0$ an M -layer system of dipolar bosons will crystallize at the critical density $290/M^5$.

Threshold density

The dipolar interlayer potential

$$V_{\text{int}}(r, l) = d^2 \frac{(r^2 - 2l^2 h^2)}{(r^2 + l^2 h^2)^{5/2}}, \quad l = 1, 2, \dots, M-1, \quad (13)$$

is anisotropic. It is attractive for small values of r but repulsive for large values of r , where r is the in-plane distance between dipoles. Consider an M -layer system of dipolar bosons in a chain phase. Now, we ask ourselves what is the threshold distance r_t between a dipole on the first layer and a dipole on the last layer, and in a next chain such that the dipolar interlayer potential is zero. This threshold distance r_t can be obtained from Eq. (13)

$$d^2 \frac{r_t^2 - 2(M-1)^2 h^2}{(r_t^2 + (M-1)^2 h^2)^{5/2}} = 0, \quad (14)$$

with $l = M-1$. Now we solve for r_t

$$r_t^2 = 2(M-1)^2 h^2. \quad (15)$$

In Fig. 5 we show the interlayer potential $V_{\text{int}}(r, M-1)$ as a function of r/r_0 for different values of the number

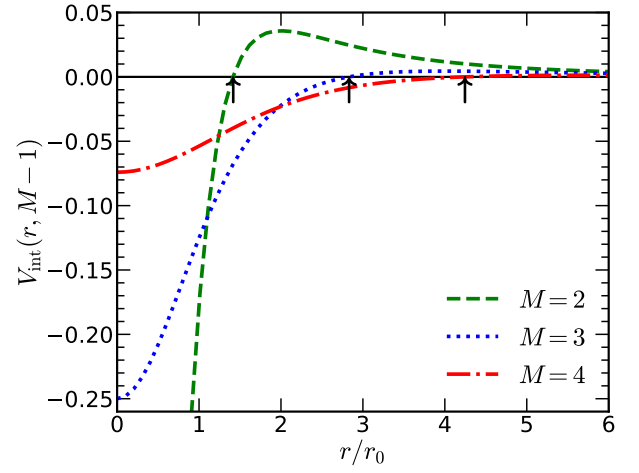


FIG. 5. Interlayer potential $V_{\text{int}}(r, M-1)$ as a function of r/r_0 for different values of the number of layers M , with $h/r_0 = 1.0$. The arrows show the positions of the threshold distances r_t for $M = 2, 3$ and 4 .

of layers M , with $h/r_0 = 1.0$. The threshold distances r_t are the points where the potential crosses the horizontal axis. The values of r_t are indicated by arrows in Fig. 5.

Now, the mean-inter-particle distance in one layer is proportional to

$$\langle r/r_0 \rangle \sim \frac{1}{\sqrt{nr_0^2/M}} \rightarrow \frac{nr_0^2}{M} \sim \frac{1}{\langle r/r_0 \rangle^2}. \quad (16)$$

From the Eq. (15) and Eq. (16) we obtain the threshold density n_t , which satisfies Eq. (14)

$$n_t r_0^2 = \frac{M}{2(M-1)^2 (h/r_0)^2}. \quad (17)$$

The threshold density Eq. (17) is an approximation. Densities larger than the threshold density $n_t r_0^2$ (attractive interlayer potential) will favor the formation of a gas phase and lower densities than the threshold density (repulsive interlayer potential) will favor the formation of the ordered phases, either solid or chains.

Finite size effects

In two dimensions, the dipolar potential is a quasi-long ranged one, therefore its truncation at $L/2$ produces significant finite-size corrections. The average energy E_{int} of the interaction potential $V(r)$ which is a two-body operator, can be expressed in terms of the pair distribution function $g(r)$ as

$$\frac{E_{\text{int}}}{N} = \frac{1}{2n} \int_0^\infty V(r)g(r)dr. \quad (18)$$

Applied to the multilayer geometry, the finite-size effects can be significantly diminished by adding the tail energy,

$$\frac{E_{\text{tail}}(n, L)}{L^2} = \int_{L/2}^{\infty} \left[\frac{M}{2} \frac{d^2}{r^3} g_{\sigma\sigma}(r) + \frac{M(M-1)}{2} \frac{d^2(r^2 - 2h^2)}{(r^2 + h^2)^{5/2}} g_{\sigma\sigma'}(r) \right] dr \quad (19)$$

The intraspecies and interspecies pair distribution functions are denoted by $g_{\sigma\sigma}(r)$ and $g_{\sigma\sigma'}(r)$, respectively. An approximate value of the tail energy (19) is obtained by ignoring correlations at large distances, $g_{\sigma\sigma}(r) \rightarrow n_{\sigma}^2$ and $g_{\sigma\sigma'}(r) \rightarrow n_{\sigma}n_{\sigma'}$, which leads to

$$\frac{E_{\text{tail}}}{N} = \frac{2\pi d^2 n^{3/2}}{M\sqrt{N}} + \frac{2\pi d^2 (M-1)N}{M(4h^2 + N/n)^{3/2}}. \quad (20)$$

In Fig. 6, we show two examples of the finite-size study for the energy. In it, we consider solid and chain phases. Notice that the addition of the tail energy (20) to the DMC data allows to significantly reduce the finite-size dependence. After adding the tail energy E_{tail} to the DMC energy E_{DMC} , we extrapolate the energy $E(N) = E_{\text{DMC}} + E_{\text{tail}}$ to the thermodynamic limit value E_{th} using the fitting formula

$$E(N) = E_{\text{th}} + \frac{C}{\sqrt{N}}, \quad (21)$$

where C is a fitting parameter. For both phases we observe that the energy dependence on the number of particles scales as $1/\sqrt{N}$, contrary to the law $1/N$, usual for fast decaying potentials. We find that our fitting function describes well the finite-size dependence.

The number of particles used in this study ranges from $N = 48$ up to $N = 224$. All the results of the energy reported in our work are corrected to the thermodynamic limit using this functional law. The same procedure is repeated for all the system parameters for the gas, chains, and solid phases.

In Fig. 7 we show the energies of a gas, solid and chains for $M = 4$, $h/r_0 = 0.6$ y $nr_0^2 = 0.4$. The energies are extrapolated to the thermodynamic limit by using the empirical law $E(N) = E_{\text{th}} + C/N^{1/2}$, with C a fitting parameter, and we have added the tail energy to reduce the finite-size effects. For the particular values shown in the figure, the chain phase is energetically favorable compared to the gas and solid phases.

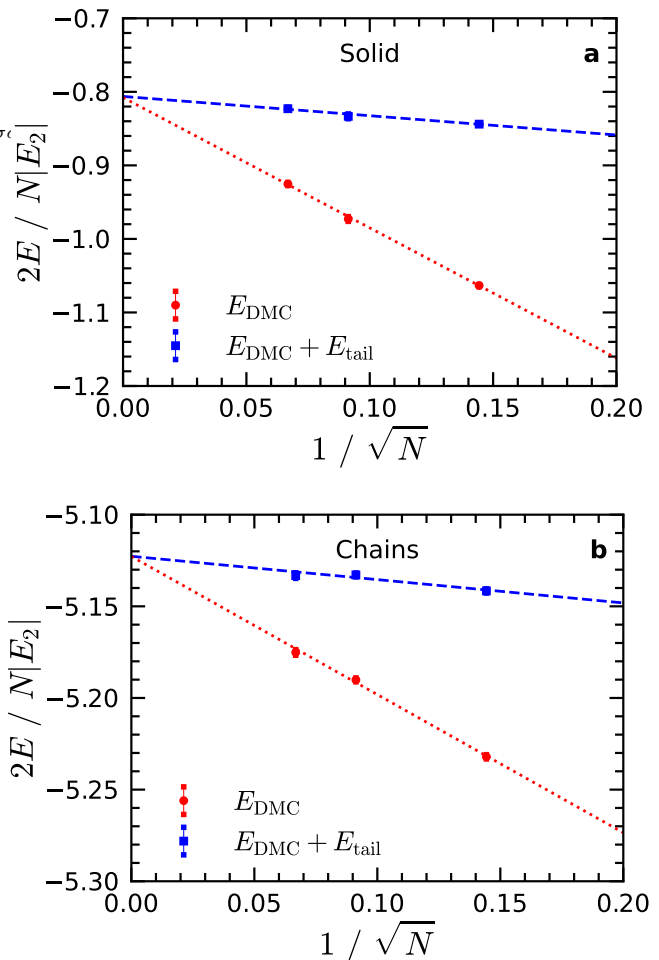


FIG. 6. Examples of the finite-size dependence for the energy in the solid (a) and chain (b) phases. Solid phase parameters: $nr_0^2 = 0.4$, $M = 4$, and $h/r_0 = 0.5$. Chain phase parameters: $nr_0^2 = 0.01$, $M = 4$, and $h/r_0 = 0.9$. Symbols, DMC energy and DMC energy with added the tail energy; curves, fit $E_{\text{th}} + C/\sqrt{N}$.

[1] A. Macia, J. Sánchez-Baena, J. Boronat, and F. Mazzanti, *Phys. Rev. Lett.* **117**, 205301 (2016).
 [2] R. N. Bisset, R. M. Wilson, D. Baillie, and P. B. Blakie, *Phys. Rev. A* **94**, 033619 (2016).
 [3] D. Baillie, R. M. Wilson, R. N. Bisset, and P. B. Blakie, *Phys. Rev. A* **94**, 021602(R) (2016).
 [4] L. Tanzi, E. Lucioni, F. Famà, J. Catani, A. Fioretti, C. Gabbanini, R. N. Bisset, L. Santos, and G. Modugno, *Phys. Rev. Lett.* **122**, 130405 (2019).

[5] F. Böttcher, M. Wenzel, J.-N. Schmidt, M. Guo, T. Langen, I. Ferrier-Barbut, T. Pfau, R. Bombín, J. Sánchez-Baena, J. Boronat, and F. Mazzanti, *Phys. Rev. Res.* **1**, 033088 (2019).
 [6] H. Kadau, M. Schmitt, M. Wenzel, C. Wink, T. Maier, I. Ferrier-Barbut, and T. Pfau, *Nature* **530**, 194 (2016).
 [7] M. Schmitt, M. Wenzel, F. Böttcher, I. Ferrier-Barbut, and T. Pfau, *Nature* **539**, 259 (2016).
 [8] I. Ferrier-Barbut, H. Kadau, M. Schmitt, M. Wenzel, and T. Pfau, *Phys. Rev. Lett.* **116**, 215301 (2016).
 [9] L. Chomaz, S. Baier, D. Petter, M. J. Mark, F. Wächtler, L. Santos, and F. Ferlaino, *Phys. Rev. X* **6**, 041039 (2016).
 [10] D. H. J. O'Dell, S. Giovanazzi, and G. Kurizki, *Phys. Rev. Lett.* **90**, 110402 (2003).
 [11] L. Santos, G. V. Shlyapnikov, and M. Lewenstein, *Phys. Rev. Lett.* **90**, 250403 (2003).
 [12] L. Chomaz, R. M. van Bijnen, D. Petter, G. Faraoni, S. Baier, J. H. Becher, M. J. Mark, F. Wächtler, L. Santos, and F. Ferlaino, *Nature physics* **14**, 442 (2018).

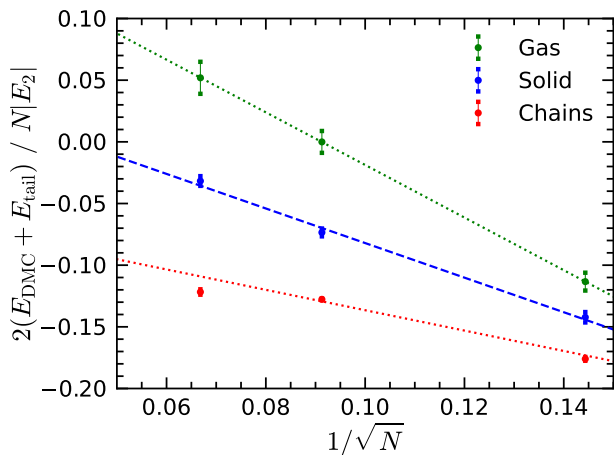


FIG. 7. Example of the chain phase being energetically favorable compared to the gas and solid phases. Phase parameters: $M = 4$, $h/r_0 = 0.6$ y $nr_0^2 = 0.4$. Symbols, DMC energy with added the tail energy; curves, fit $E_{\text{th}} + C/\sqrt{N}$.

- [13] J.-S. You and D.-W. Wang, *New Journal of Physics* **16**, 073041 (2014).
- [14] J.-R. Li, J. Lee, W. Huang, S. Burchesky, B. Shteynas, F. Ç. Top, A. O. Jamison, and W. Ketterle, *Nature* **543**, 91 (2017).
- [15] J. Léonard, A. Morales, P. Zupancic, T. Esslinger, and T. Donner, *Nature* **543**, 87 (2017).
- [16] L. Chomaz, D. Petter, P. Ilzhöfer, G. Natale, A. Trautmann, C. Politi, G. Durastante, R. M. W. van Bijnen, A. Patscheider, M. Sohmen, M. J. Mark, and F. Ferlaino, *Phys. Rev. X* **9**, 021012 (2019).
- [17] F. Böttcher, J.-N. Schmidt, M. Wenzel, J. Hertkorn, M. Guo, T. Langen, and T. Pfau, *Physical Review X* **9**, 011051 (2019).
- [18] E. Wigner, *Phys. Rev.* **46**, 1002 (1934).
- [19] D.-W. Wang, M. D. Lukin, and E. Demler, *Phys. Rev. Lett.* **97**, 180413 (2006).
- [20] B. Hammond, W. Lester, and P. Reynolds, *Monte Carlo Methods in Ab Initio Quantum Chemistry*, Lecture and Course Notes In Chemistry Series (World Scientific, 1994).
- [21] J. Toulouse, R. Assaraf, and C. J. Umrigar, “Introduction to the variational and diffusion Monte Carlo methods,” (2015), [arXiv:1508.02989 \[physics.chem-ph\]](https://arxiv.org/abs/1508.02989).
- [22] J. Boronat and J. Casulleras, *Phys. Rev. B* **49**, 8920 (1994).
- [23] D. Ceperley, *Reviews in Mineralogy & Geochemistry - REV MINERAL GEOCHEM* **71**, 129 (2010).
- [24] A. Macia, G. E. Astrakharchik, F. Mazzanti, S. Giorgini, and J. Boronat, *Phys. Rev. A* **90**, 043623 (2014).
- [25] G. E. Astrakharchik, R. E. Zillich, F. Mazzanti, and J. Boronat, *Phys. Rev. A* **94**, 063630 (2016).
- [26] G. Guijarro, G. E. Astrakharchik, and J. Boronat, *Phys. Rev. Lett.* **128**, 063401 (2022).
- [27] L. Du, P. Barral, M. Cantara, J. de Hond, Y.-K. Lu, and W. Ketterle, “Atomic physics on a 50 nm scale: Realization of a bilayer system of dipolar atoms,” (2023).
- [28] M. Lu, N. Q. Burdick, S. H. Youn, and B. L. Lev, *Phys. Rev. Lett.* **107**, 190401 (2011).
- [29] A. Trautmann, P. Ilzhöfer, G. Durastante, C. Politi, M. Sohmen, M. J. Mark, and F. Ferlaino, *Phys. Rev. Lett.* **121**, 213601 (2018).
- [30] T. Takekoshi, L. Reichsöllner, A. Schindewolf, J. M. Hutson, C. R. Le Sueur, O. Dulieu, F. Ferlaino, R. Grimm, and H.-C. Nägerl, *Phys. Rev. Lett.* **113**, 205301 (2014).
- [31] P. K. Molony, P. D. Gregory, Z. Ji, B. Lu, M. P. Köppinger, C. R. Le Sueur, C. L. Blackley, J. M. Hutson, and S. L. Cornish, *Phys. Rev. Lett.* **113**, 255301 (2014).
- [32] M. Guo, B. Zhu, B. Lu, X. Ye, F. Wang, R. Vexiau, N. Bouloufa-Maafa, G. Quéméner, O. Dulieu, and D. Wang, *Phys. Rev. Lett.* **116**, 205303 (2016).
- [33] M. Guo, X. Ye, J. He, G. Quéméner, and D. Wang, *Phys. Rev. A* **97**, 020501(R) (2018).
- [34] V. Cikojević, L. V. c. v. Markić, G. E. Astrakharchik, and J. Boronat, *Phys. Rev. A* **99**, 023618 (2019).
- [35] L. Parisi, G. E. Astrakharchik, and S. Giorgini, *Phys. Rev. Lett.* **122**, 105302 (2019).
- [36] T. Comparin, R. Bombín, M. Holzmann, F. Mazzanti, J. Boronat, and S. Giorgini, *Phys. Rev. A* **99**, 043609 (2019).
- [37] G. Guijarro, G. E. Astrakharchik, J. Boronat, B. Bazak, and D. S. Petrov, *Phys. Rev. A* **101**, 041602 (2020).
- [38] L. A. P. Ardila, G. E. Astrakharchik, and S. Giorgini, *Phys. Rev. Research* **2**, 023405 (2020).
- [39] R. Bombín, T. Comparin, G. Bertaina, F. Mazzanti, S. Giorgini, and J. Boronat, *Phys. Rev. A* **100**, 023608 (2019).
- [40] R. Bombin, J. Boronat, and F. Mazzanti, *Phys. Rev. Lett.* **119**, 250402 (2017).
- [41] O. A. Rodríguez-López, M. A. Solís, and J. Boronat, *Phys. Rev. A* **103**, 013311 (2021).
- [42] J. Sánchez-Baena, J. Boronat, and F. Mazzanti, *Phys. Rev. A* **98**, 053632 (2018).
- [43] L. Reatto and G. V. Chester, *Phys. Rev.* **155**, 88 (1967).
- [44] C. Cazorla and J. Boronat, *Rev. Mod. Phys.* **89**, 035003 (2017).
- [45] G. Guijarro, *Quantum Monte Carlo study of few- and many-body Bose systems in one and two dimensions*, Ph.D. thesis, Universitat Politècnica de Catalunya (2020).
- [46] G. E. Astrakharchik, J. Boronat, I. L. Kurbakov, and Y. E. Lozovik, *Phys. Rev. Lett.* **98**, 060405 (2007).